DYNAMIC ANALYSIS OF STEEL MAST UNDER SOME ENVIRONMENTAL UNCERTAINTIES

R. Bredow [1] **M. Kamiński** [2]
[1] PhD Candidate, Department of Structural Mechanics, Łódź University of Technology, POLAND,
Rafal.Bredow@dokt.p.lodz.pl
[2] Professor, Department of Structural Mechanics, Łódź University of Technology, POLAND,
Marcin.Kaminski@p.lodz.pl

ABSTRACT: A concise and factual abstract is required. The abstract should state briefly the purpose of the research, the principal results and major conclusions. An abstract is often presented separately from the article, so it must be able to stand alone. For this reason, references should be avoided, but if essential, then cite the author(s) and year(s). Also, non-standard or uncommon abbreviations should be avoided, but if essential they must be defined at their first mention in the abstract itself.

Keywords: generalized stochastic perturbation technique, Stochastic Finite Element Method, reliability analysis, structural mechanics.

1. INTRODUCTION

The aim of this work is to analyse behaviour of some steel mast under dynamic excitation of the given wind spectrum including also uncertain temperature load and further to contrast two different Finite Element Method solvers of equations of motion integration.

The exemplary structure taken into account is a steel mast plsced in Zygry. Mast structure features the height equal to 198,0 meters. The mast shaft has been designed with the use of S235J2 steel in form of three-walled lattice with side width equal to 130,0 cm. The leg members have been modelled as round pipes with diameter of 168,3 mm and with the cross-section wall thickness varying along a height of this structure. The mast face lacings have been introduced as the round pipes of diameter 63,5 mm and also varying cross-section wall thicknesses. The mast guys have been attached to the shaft at following heights: 60,0 m, 120,0 m and 180,0 m with the inclination angle equal to about 45°. A spiral strand steel rope 1x37 with the diameter of 32,0 mm has been applied having mean strength of 1960 MPa and elasticity modulus of 150GPa. An initial tension of the guys has been set by pre-shortening equal to 11,0 cm, 22,0 cm and 31,0 cm correspondingly for consecutive attachment levels with ascending order starting from the bottom. A general geometry of this mast has been presented in Figure 1.1a. Geometry of shaft has been presented in Figure 1.1b.

Environmental uncertainty has been expressed by the Gaussian temperature load. Positive and negative temperature loads have been considered dependingly on which of these two contributes more significantly to structural safety reduction regarding some principal state variables. Positive temperature load has been introduce within a range of -10°C to +40°C when negative temperature load has been described within

a range of -50°C to ±0°C. Computations have been performed regarding both types of temperature load and repeated 11 times dividing both ranges of temperature load into ±5°C interval. The assumption has been made that the temperature applied to structure acts equally and no temperature fluctuations regarding height of the structure has been considered.
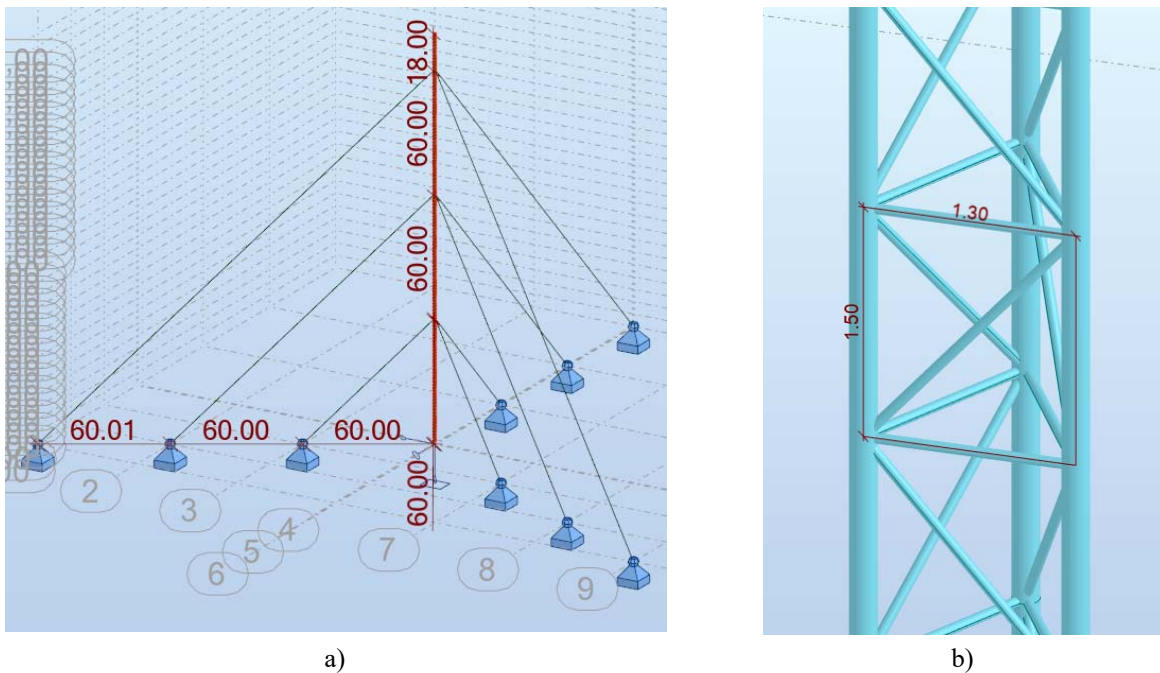

Fig. 1.1. Mast geometry: a) general geometry, b) mast shaft geometry.

Computations have been performed regarding both types of temperature load and repeated 11 times dividing both ranges of temperature load into ±5°C temperature interval. The assumption has been made that the temperature applied to structure acts equally and no temperature fluctuations regarding height of the structure has been considered. Principal state variables have been identified as stress of the main legs and of the face lacing referring to single structural elements of the mast. Global horizontal displacement and rotation of the entire structure top have been also considered for this purpose. Several series of numerical simulations with the Finite Element Method system have been performed assuming specific dynamic action of the wind load (see Fig. 1.2). This wind load has been modelled according to the Eurocode 1 guidelines (1) for towers, chimneys and masts including an effect of local wind gusts (2, 3, 4). Dynamic analysis of the wind influence on this structure has been performed in 10 minutes time interval.
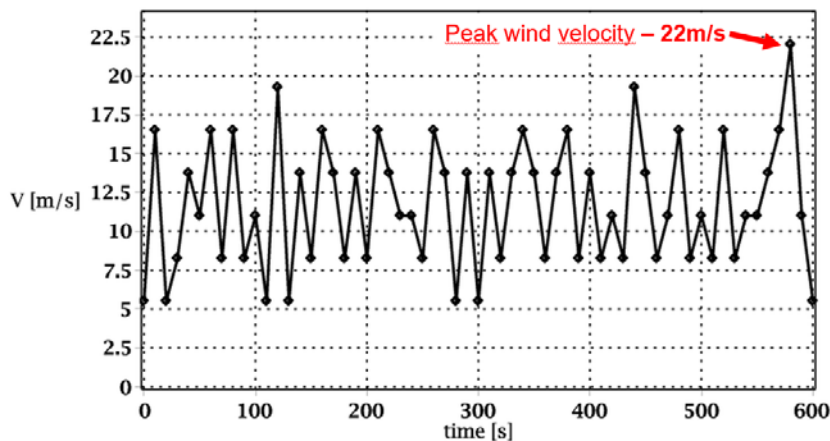

Fig. 1.2. History of wind load introduced into calculations.

Lightweight Structures in Civil Engineering. Contemporary Problems

This includes some wind action applied to the entire structure (see Fig. 1.3a) and some patch loads describing additional wind gusts along the height of the structure (see Fig. 1.3b).
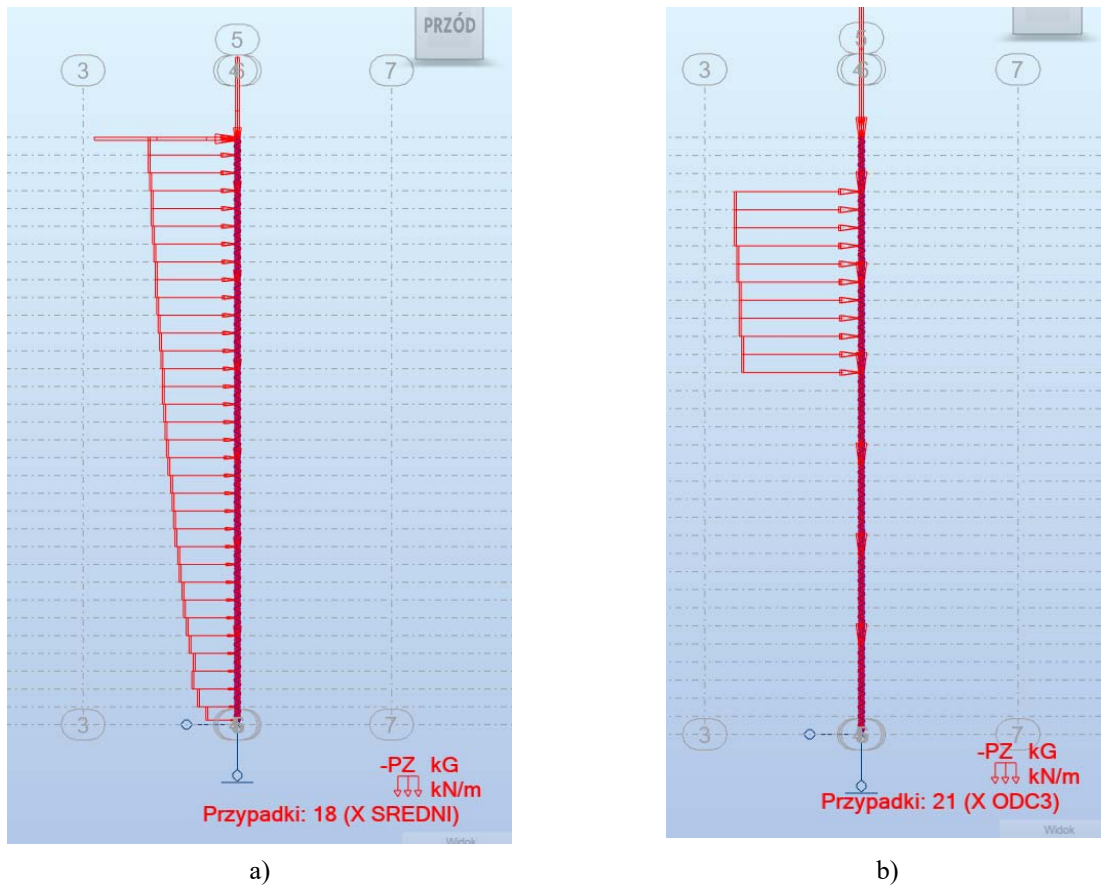

a)   b)

Fig. 1.3. Exemplary wind load acting along X-axis of global coordinate system: a) mean load, b) patch load.

2. NUMERICAL SOLUTION

Numerical solution for each computational case study has been performed in Autodesk Robot Structural Analysis (ARSA) using non-linear dynamic analysis option based on the Broyden-Fletcher-Goldfarb-Shanno (BFGS) algorithm. Hilber-Hughes-Taylor (HHT) solver has been applied in order to integrate equations of motion (5). It is based upon the following approximation of the structural displacements and velocities:

$$\begin{cases} x_{i+1} = x_i + \Delta t \cdot \dot{x}_i + \left(1/2 - \beta\right) \cdot \left(\Delta t\right)^2 \cdot \ddot{x}_i, \\ \qquad \dot{x}_{i+1} = \dot{x}_i + \left(1 - \gamma\right) \cdot \Delta t \cdot \ddot{x}_i. \end{cases} \tag{2.1}$$

Additionally, the HHT solver has been contrasted with the results achieved by Newmark method (6) and exemplary results have been presented in Figure 2.1.
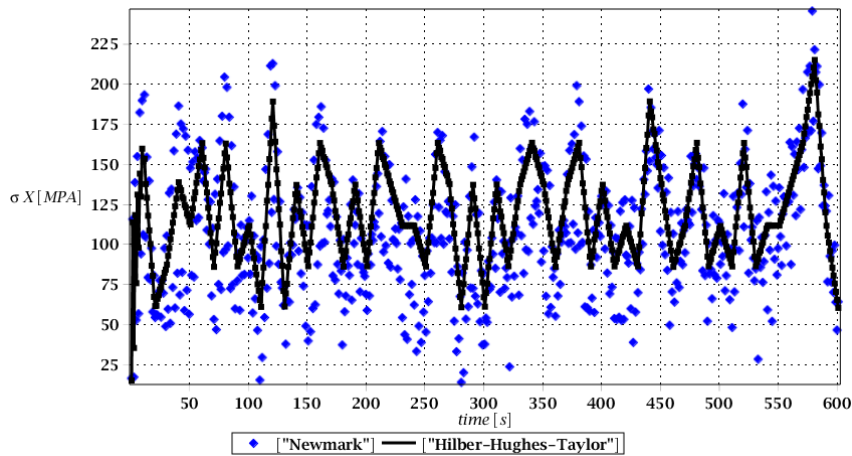
Fig. 2.1. History of normal stresess in main leg under dynamic wind excctitation
obtained using the HHT and Newmark method.

This figure documents very well that the Newmark algorithm results in relatively larger variations of the given stress about the value relevant to the static equilibrium, while the HHT series is obtained in a quite regular pattern.

At this point it has to be mentioned that Autodesk Robot Structural Analysis does not calculate effective stress in beam elements. The index of share of normal stress in Huber-Mises effective stress has been investigated in order to check whereas there is a necessity to calculate an effective stress in each time step manually for main legs and face lacing elements. In order to pursue such investigation, author checked the effective stress of elements by finding elements in which normal or shear stress calculated by ROBOT was the greatest among the entire structure and time of analysis. Products of solving equations of motion indicates that those elements are mainly stressed by axial force and some bending moments. Shear forces and torsional moment are of the minor interest as those figures are mainly lesser by three orders of magnitude comparing to normal force. Nevertheless effective stress has been calculated by following Huber-Mises hypothesis of effective stress. Normal stress has been calculated as a product of axial force and bending moments acting on a cross section of element (see Fig 2.2a.). Total shear stress has been calculated as a product of vector aggregation performed on shear stress generated by shear forces and by torsional moment (see Fig 2.2b.). Taking into account abovementioned procedure, effective stress has been calculated for main leg and face lacing truss. This calculations has been performed by a deterministic approach as it is recommened by currently valid engineering guidelines (i.e. Eurocodes). In some future research on the other hand, some probabilistic approach might be worth taking into account regarding such a cross-sectional stress distribution analysis. Exemplary calculations performed for main leg element are being presented below. Cross sectional properties:

$$r = 8.4cm,$$
$$A = 58.9cm^2,$$
$$J_y = J_z = J_1 = 1810cm^4,$$

$$J_0 = \frac{4A_0{}^2}{\oint \frac{ds}{\delta}} = \frac{4 \cdot \left(\pi \cdot (8.4cm)^2 \right)^2}{2\pi \cdot 8.4cm} = 3724.07cm^4.$$

(2.2)

Lightweight Structures in Civil Engineering. Contemporary Problems

Internal forces have been determined consecutively and they equal in turn:

$$N_{Ed} = -1089.19kN,$$
$$T_{Ed} = -0.05kNm,$$
$$M_{y.Ed} = 4.84kNm,$$
$$M_{z.Ed} = -3.88kNm,$$
$$V_{y.Ed} = 0.97kNm,$$
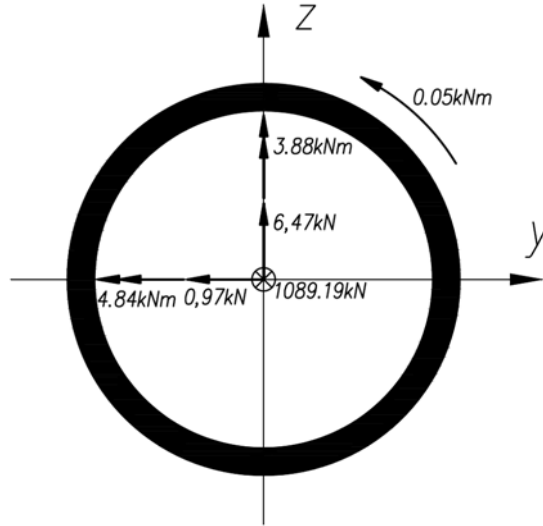$$V_{z.Ed} = -6.47kN.$$

(2.3)

Fig. 2.2. Load acting on cross-section of chosen main leg element.

Utilizing bi-simmetrical properties of cross section, normal stress can be easily calculated in tilted coordinate system. Effective bending moment might be represented as:

$$M_{Ed} = \sqrt{M_{y.Ed}{}^2 + M_{z.Ed}{}^2} = \sqrt{4.84^2 + 3.88^2}\,kNm = 6.20kNm.$$

(2.4)

Resulting normal stress is then calculated respectively:

$$\sigma_A = \frac{-N_{Ed}}{A} + \frac{M_{Ed}}{J_1} \cdot \rho = \frac{-1089.19kN}{58.9 \cdot 10^{-4}m^2} + \frac{-6.20kNm}{1810 \cdot 10^{-8}m^4} \cdot 84 \cdot 10^{-3}m = -213.695MPa.$$

(2.5)

Shear stress has been calculated in point A, which corresponds to greatest normal stress and considering relatively small shear stress, point A describes greatest effective stress as well.

$$\tau_{mean.Z} = \frac{V_{z.Ed}}{A} = \frac{6.47kN}{58.9 \cdot 10^{-4}m^2} = 1.098MPa.$$

(2.6)

$$\tau_{xz}{}^A = \frac{4}{3} \cdot \tau_{mean.Z} \cdot \cos(51.26°) = 0.916MPa.$$

(2.7)

$$\tau_{mean.Y} = \frac{V_{y.Ed}}{A} = \frac{0.97kN}{58.9 \cdot 10^{-4}m^2} = 0.165MPa.$$

(2.8)

$$\tau_{xy}{}^{A} = \frac{4}{3} \cdot \tau_{mean.Y} \cdot \sin(51.26°) = 0.172 MPa. \tag{2.9}$$

$$\tau_{T.z}{}^{A} = \tau_{T}{}^{A} = \frac{T_{Ed}}{W_0} \cdot \cos(51.26°) = \frac{0.05 kNm}{532.01 \cdot 10^{-6} m^3} \cdot \cos(51.26°) = 0.0588 MPa. \tag{2.10}$$

$$\tau_{T.y}{}^{A} = \tau_{T}{}^{A} = \frac{T_{Ed}}{W_0} \cdot \sin(51.26°) = \frac{0.05 kNm}{532.01 \cdot 10^{-6} m^3} \cdot \sin(51.26°) = 0.0733 MPa. \tag{2.11}$$

$$\overline{\tau}_{y}{}^{A} = \overline{\tau}_{xy}{}^{A} + \overline{\tau}_{T.y}{}^{A} = 0.172 MPa + 0.0733 MPa = 0.2453 MPa. \tag{2.12}$$

$$\overline{\tau}_{z}{}^{A} = \overline{\tau}_{xz}{}^{A} + \overline{\tau}_{T.z}{}^{A} = 0.0588 MPa + 0.916 MPa = 0.9748 MPa. \tag{2.13}$$
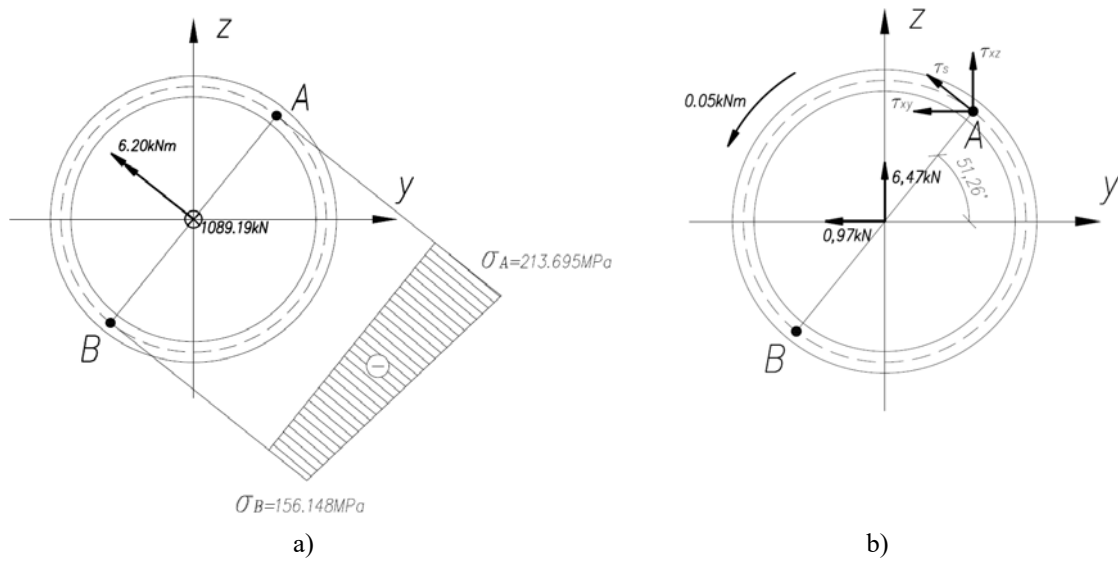
Fig. 2.3. Stress generated by internal forces: a) normal stress,
b) shear stress as a product of vector-aggregation.

Finally, the Huber-Mises effective stress in point A:

$$\sigma_{red}{}^{HA} = \sqrt{\left(\sigma^A\right)^2 + 3\left(\tau^A\right)^2} = \sqrt{213.695^2 + 3 \cdot 1.01^2} MPa = 213.702 MPa. \tag{2.14}$$

Share index of normal stress to effective stress has been described as:

$$\frac{\left|\sigma^A\right|}{\sigma_{red}{}^{HA}} = \frac{213.695 MPa}{213.702 MPa} = 0.99997 = 99.997\%. \tag{2.15}$$

Comparison of a normal stress to effective stress shows that the influence of shear stress might be neglected. Simmilar calculations and conclusions has been drawn from analysis of stress state of face lacing elements. This brings the conclusion that calculating effective stress every time step of calculations can be neglected and normal stress can be taken as a representative instead.

Discrete results of the resulting extreme stresses and displacements have been saved for any second of FEM simulations, where every save step has been subdivided into 10 time steps giving as a result computational time step equal to Δt=0.10 s. This calculus procedure has been repeated for 11 series of uniform temperature

load within a range of -50 °C up to +40 °C. A set of 600 discrete values of stresses and displacements computed for several series of the FEM tests was the basis to carry out Structural Response Function estimation in a form of the 11th order polynomial (or less). Polynomials have been fitted by the Weighted Least Squares Method in which the weighing function has been assumed as a triangular one. Structure Response Function (SRF) accuracy has been adjusted by the mean square root error minimization criterium as well as controlling whether over-fitting problem occurs. The SRF has been recovered for each random state variable separately (leg stress, face lacing stress, horizontal displacement and rotation) at any save step using both solvers (HHT and Newmark) giving as a result 4x600=2400 SRFs. These SRFs are analytical functions of the external temperature, which is assumed to be Gaussian variable. It has to be noted that polynomial order has been established once for all series of the SRFs that describe one of four state variables i.e. horizontal displacement. This means that all 600 SRFs associated with horizontal displacement in subsequent save steps of movement are described by polynomials of the same order.

3. PROBABILISTIC ANALYSIS

The generalized Stochastic Perturbation Technique (SPT) (7) has been introduced in order to compute the basic probabilistic characteristics of the structural response, where Monte Carlo Simulation (MCS) and Semi-Analytical Method (SAM) have been chosen as the reference techniques (8, 9, 10). Time fluctuations of the expected values, variances, skewness, kurtosis and coefficient of variation for the extreme values of normal stresses in the main legs have been presented in Figures (3.1-3.16), correspondingly.
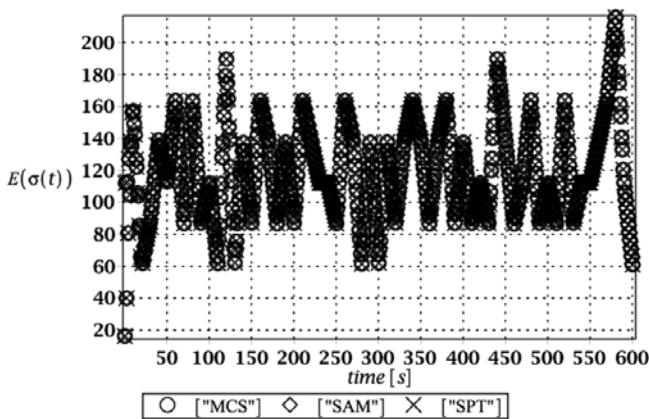

Fig. 3.1. History of expected value for normal stress in main legs.
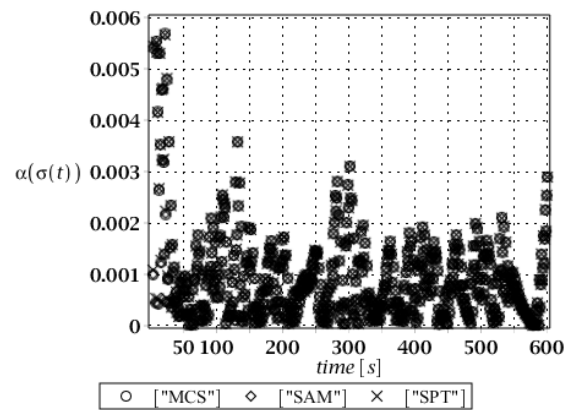

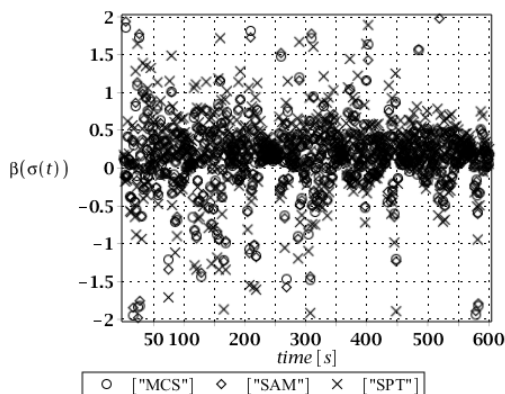Fig. 3.2. History of the coefficient of variation for normal stress in main legs.

Fig. 3.3. History of the skewness for normal stress in main legs.
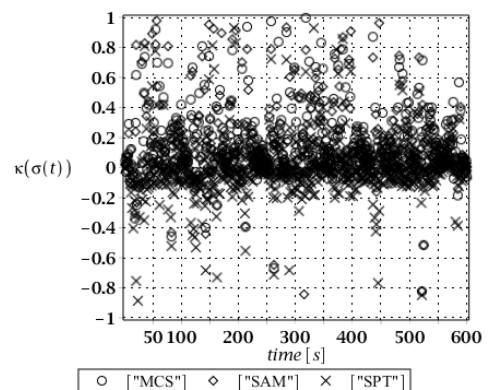

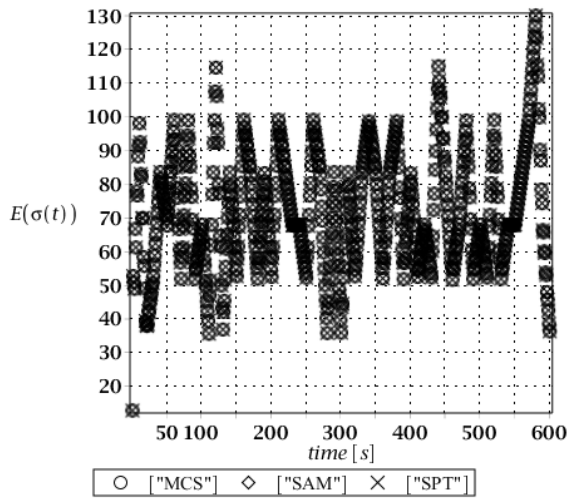Fig. 3.4. History of the kurtosis for normal stress in main legs.

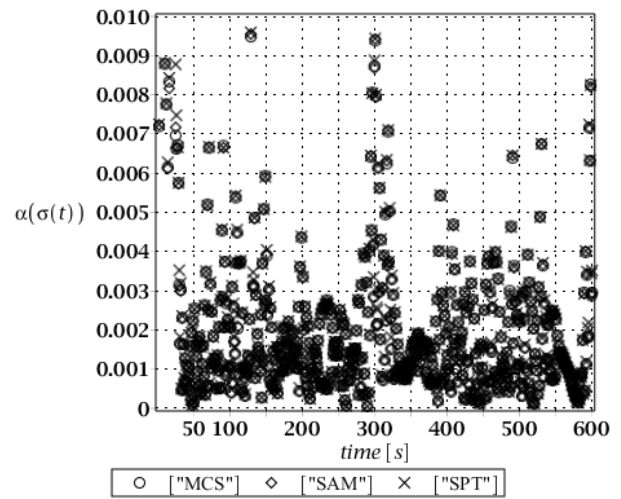Fig. 3.5. History of the expected values of stress in face lacing.

Fig. 3.6. History of coefficient of variation of stress in face lacing.
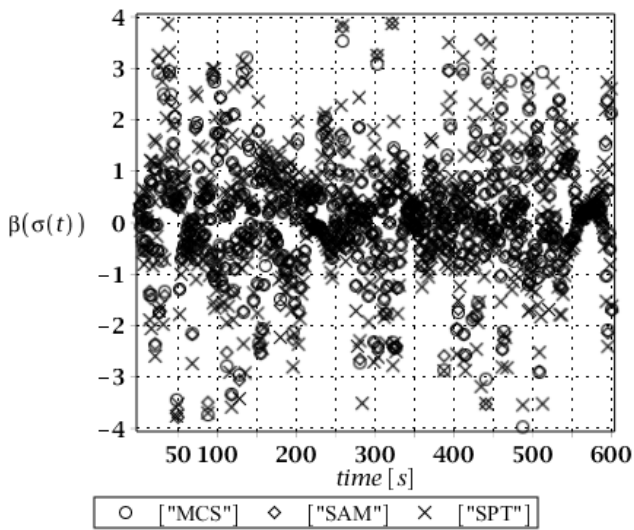

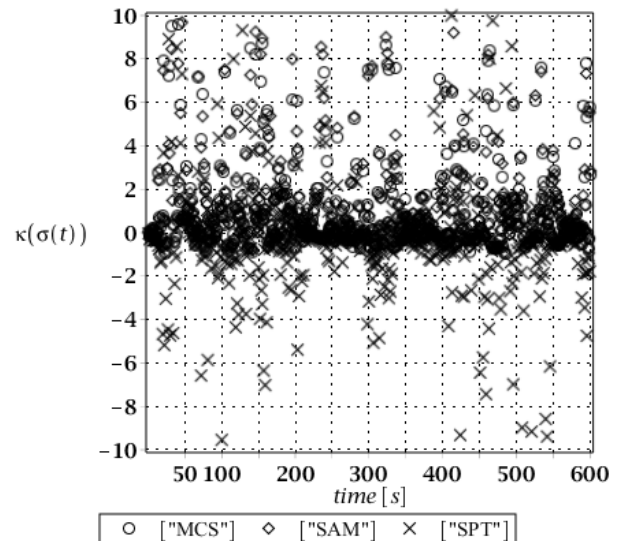Fig. 3.7. History of skewness of stress in face lacing.

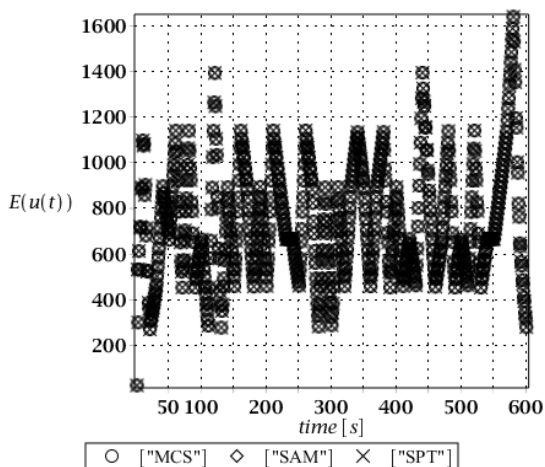Fig. 3.8. History of skewness of stress in face lacing.

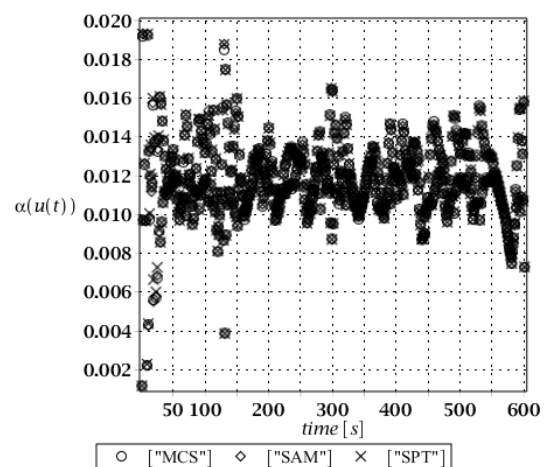Fig. 3.9. History of expected values of horizontal displacement.

Fig. 3.10. History of coefficient of variation of horizontal displacement.
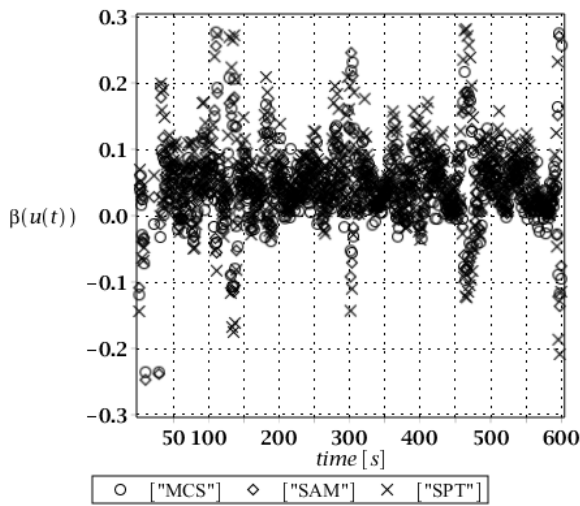
Fig. 3.11. History of skewness of horizontal displacement.
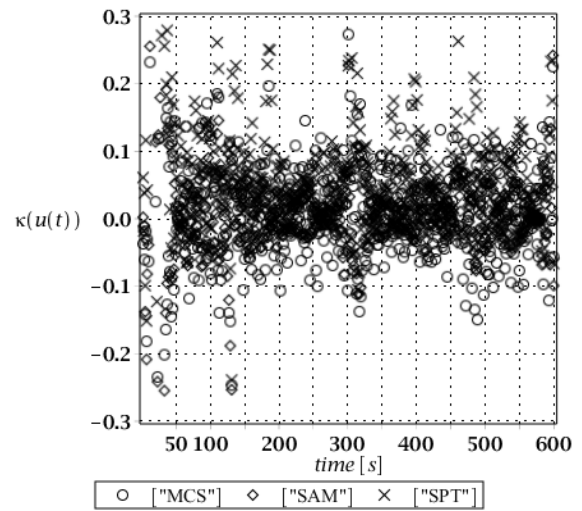

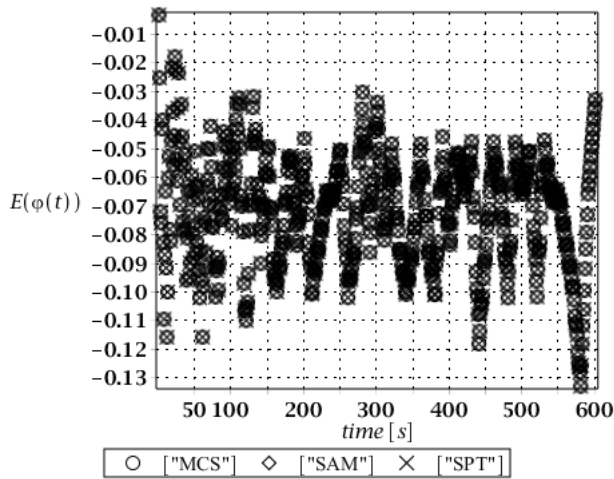Fig. 3.12. History of kurtosis of horizontal displacement.

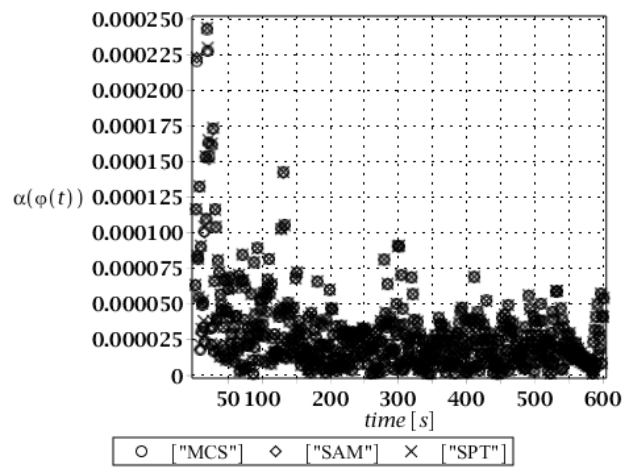Fig. 3.13. History of expected values of rotation.

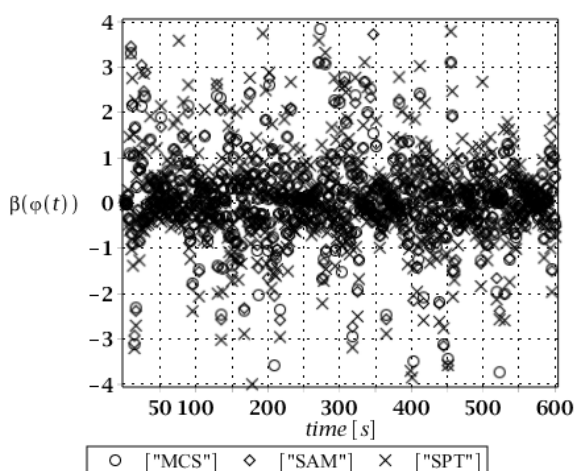Fig. 3.14. History of coefficient of variation of rotation.
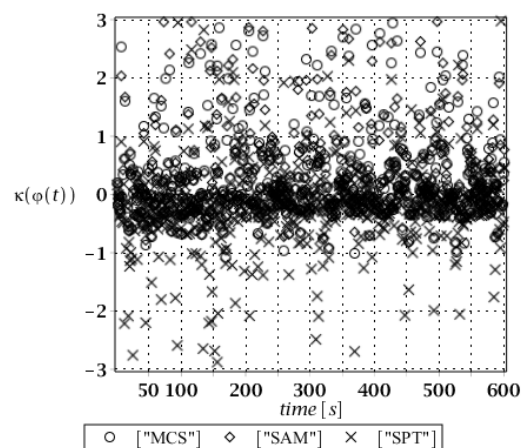

Fig. 3.15. History of skewness of rotation.

Fig. 3.16. History of kurtosis of rotation.

4. CONCLUDING REMARKS

A very general conclusion, which can be drawn from these results is a good coincidence of all three probabilistic numerical methods, which taking into account nonlinear problem with large deformations including dynamic excitation is not trivial. Numerical results obtained here, and especially the first two probabilistic moments, may be directly used in stochastic reliability assessment according to the statements proposed in Eurocode 0. Finally, one can conclude that external temperature uncertainty has rather limited importance while dynamic stresses fluctuations are under consideration and cannot affect remarkably the resulting reliability index.

REFERENCES

Eurocode 1: Actions on structures – Part 1-4: General actions – Wind actions – European Committee for Standardization, Brussels, 2010.

Eurocode 3: Design of steel structures – Part 3-1: Towers, masts and chimneys – Towers and masts – European committee for Standardization, Brussels, 2006.

Spak, K.S., Agnes, G.S., Inman, D.J. 2015. *Modeling vibration response and damping of cables and cables structures*. Journal of Sound & Vibration 336: 240-256.

Wang, L., Rega, G. 2010. *Modelling and transient planar dynamics of suspended cables with moving mass*. International Journal of Solids & Structures 47: 2733-2744.

Hilber, H.M., Hughes, T.J.R. & Taylor, R.L. 1997. *Improved Numerical Dissipation for Time Integration Algorithms in Structural Dynamics*. Earthquake Engineering & Structural Dynamics 5: 282-292.

Newmark, N.M. 1959. *A method of computation for structural dynamics*. Journal of the Engineering Mechanics Division 85 (EM3): 67-94.

Kamiński, M. The Stochastic Perturbation Method for Computational Mechanics. Chichester: Wiley.

Bredow, R. & Kamiński, M. 2021. *Computer analysis of dynamic reliability of some concrete beam structure exhibiting random damping*. International Journal of Applied Mechanics and Engineering 26(1): 45-64.

Kamiński, M. & Bredow, R. *On uncertainty analysis for overhead powerlines by the generalized stochastic perturbation technique*. Journal of Aerospace Engineering (in press).

Carassale L, Solari G. 2006. *Monte Carlo simulations of wind velocity fields on complex structures*. Journal of Wind Engineering and Industrial Aerodynamics 94: 323–339.